

Coherent X-ray scattering beamline at port 9C of Pohang Light Source II

Chung-Jong Yu,^{a*} Hae Cheol Lee,^a Chan Kim,^b Wonsuk Cha,^c Jerome Carnis,^c Yoonhee Kim,^b Do Young Noh^b and Hyunjung Kim^c

^aPohang Accelerator Laboratory, POSTECH, Pohang, Gyungbuk 790-784, Republic of Korea, ^bDepartment of Physics and Photon Science and School of Materials Science and Engineering, Gwangju Institute of Science and Technology, Gwangju 500-712, Republic of Korea, and ^cDepartment of Physics, Sogang University, Seoul 121-742, Republic of Korea. *E-mail: cju@postech.ac.kr

The coherent X-ray scattering beamline at the 9C port of the upgraded Pohang Light Source (PLS-II) at Pohang Accelerator Laboratory in Korea is introduced. This beamline provides X-rays of 5–20 keV, and targets coherent X-ray experiments such as coherent diffraction imaging and X-ray photon correlation spectroscopy. The main parameters of the beamline are summarized, and some preliminary experimental results are described.

Keywords: coherent X-ray diffraction imaging; X-ray photon correlation spectroscopy; X-ray scattering.

© 2014 International Union of Crystallography

1. Introduction

Since Sutton *et al.* (1991) observed X-ray speckles with a synchrotron X-ray source, there have been numerous studies and developments for utilizing X-ray coherence. Coherence-based techniques developed so far include X-ray photon correlation spectroscopy (XPCS) (Mochrie *et al.*, 1997; Wochner *et al.*, 2009), coherent X-ray diffraction imaging (CDI), Bragg CDI (Miao *et al.*, 1999; Chapman & Nugent, 2010; Williams *et al.*, 2003; Shapiro *et al.*, 2005) and Fourier transform holography (FTH) (Eisebitt *et al.*, 2004; Stadler *et al.*, 2008). XPCS is mainly used for studying the dynamics of materials, and CDI and FTH for static imaging. Rather recently X-ray cross-correlation analysis (Wochner *et al.*, 2009) was developed to classify the hidden local order within disorder.

Several beamlines worldwide have been used for coherent X-ray experiments: 8-ID [Advanced Photon Source (APS), USA] for XPCS, 34-ID-C (APS) for coherent X-ray scattering, BL29 (Spring-8,

Japan) for coherent X-ray optics, sector 7 (P10) (Petra III, Germany) for XPCS and CDI, I13L (Diamond, UK) for X-ray imaging and coherence, TROICA (European Synchrotron Radiation Facility, France) and so on. Pohang Accelerator Laboratory (PAL) upgraded PLS to PLS-II in 2012 increasing the electron energy from 2.5 to 3.0 GeV in the storage ring (Shin *et al.*, 2013). With this upgrade the 9C port at PLS-II was assigned for coherent X-ray experiments and has been open to domestic and international users.

2. Beamline overview

The 9C beamline at PAL is optimized to preserve the hard X-ray beam coherence from its undulator source. Fig. 1 shows a schematic diagram of the beamline. The photon source is a hybrid- and asymmetric-type in-vacuum undulator of length 1.3 m with 20 mm period and 130 poles. The magnet blocks are composed of Sm₂Co₁₇. Its

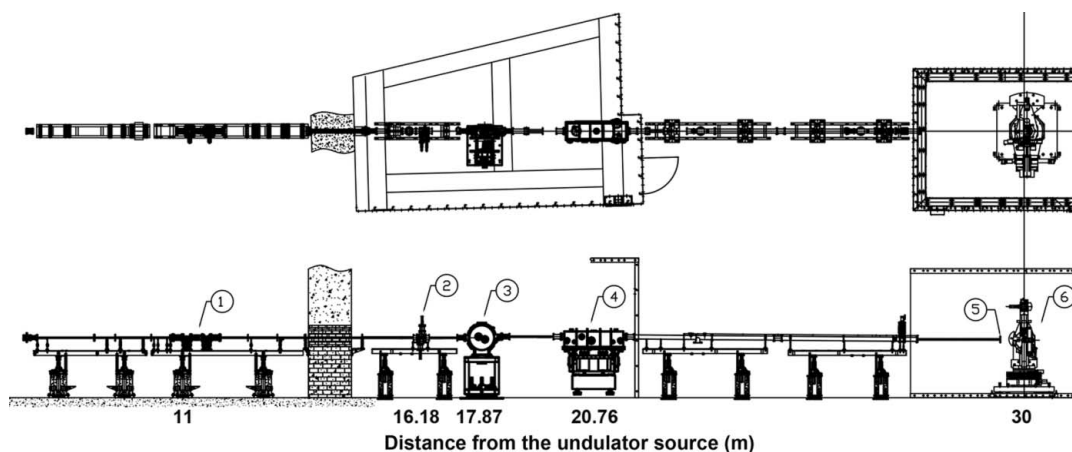


Figure 1

Layout of the 9C beamline: (1) movable masks; (2) vertical and horizontal slits; (3) Si(111) double-crystal monochromator; (4) Rh-coated focusing mirror; (5) aperture; (6) six-axis diffractometer. The drawing at the top is the top view and the drawing at the bottom is the side view of the beamline. The numbers below the main components are the distances from the undulator source in metres.

Table 1

Photon energy and highest brilliance/flux/coherent flux with corresponding undulator parameters (a target ring current of 400 mA is used).

Energy (keV)	Harmonic	Gap (mm)	K	Brilliance (flux mm ⁻² mrad ⁻²)	Flux [photons s ⁻¹ (0.1% bandwidth) ⁻¹]	Coherent flux [photons s ⁻¹ (0.1% bandwidth) ⁻¹]
6	3	5.80	1.51	9.74×10^{18}	5.24×10^{14}	1.04×10^{11}
8	3	7.60	1.10	4.93×10^{18}	2.33×10^{14}	2.96×10^{10}
10	5	5.80	1.51	4.37×10^{18}	2.19×10^{14}	1.68×10^{10}
12	7	5.01	1.73	3.37×10^{18}	1.75×10^{14}	8.99×10^9
14	7	5.80	1.51	1.95×10^{18}	9.49×10^{13}	3.82×10^9
16	9	5.19	1.68	1.57×10^{18}	7.92×10^{13}	2.36×10^9
18	9	5.80	1.51	8.71×10^{17}	4.18×10^{13}	1.03×10^9
20	11	5.31	1.64	7.22×10^{17}	3.58×10^{13}	6.94×10^8

Table 2

Main parameters of the coherent X-ray scattering beamline at PLS-II (Welnak *et al.*, 1994; Tanaka, undated).

Beamline name	Coherent X-ray scattering beamline
Port	9C
Source type	In-vacuum undulator, IVU20 (period 2 cm, gap 5–20 mm)
Mirror (toroidal)	1.1 m Si substrate with 40 nm coated Rh
Monochromator	Liquid-nitrogen-cooled DCM, Si(111)
Energy range (keV)	5–20
Σ_y/Σ_x (μm)	12/198
Σ'_y/Σ'_x (μm)	13/48
Source beam size (μm)	12 (V) × 200 (H)
Unfocused beam size (μm)	590 (V) × 2950 (H) at 30 m
Focused beam size (μm)	15 (V) × 190 (H) at 30 m
Detectors	APD, PIXIS-XO 1024B, Pilatus 1M

physical gap range is 5–20 mm, and the available X-ray energy range is 5–20 keV. The estimated source size of the photon beam is estimated to be 200 μm (H) × 12 μm (V) in FWHM (full width at half-maximum) using the *SHADOW* program (Welnak *et al.*, 1994). Figs. 2(a) and 2(b) show calculated energy and brilliance, respectively, using *SPECTRA* (Tanaka, undated) for odd harmonics *versus* the

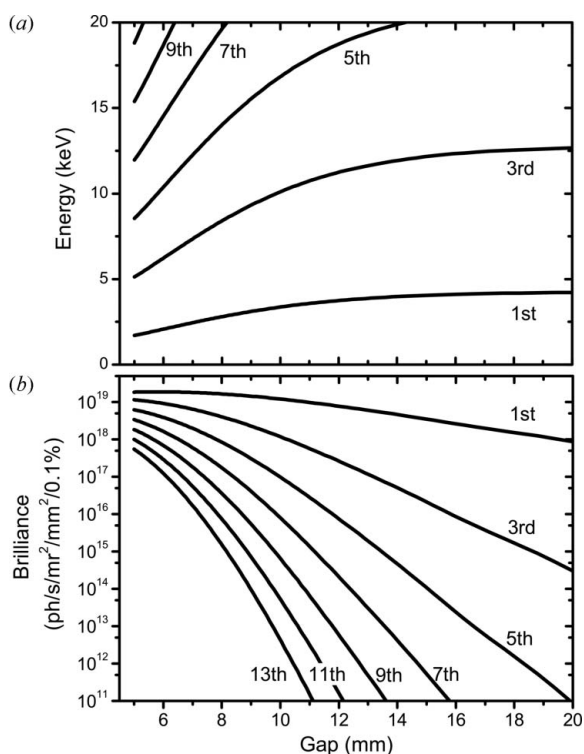


Figure 2

Calculated (a) energy and (b) brilliance curves for odd harmonics as a function of the undulator gap. (A target ring current of 400 mA is used.)

undulator gap using measured magnetic fields (e.g. 0.92 T at a gap of 5 mm) (D.-E. Kim, private communication). Using the information in Fig. 2, we summarize the highest flux values for various photon energies with corresponding undulator parameters in Table 1.

The X-ray beam as shown in Fig. 1 passes through the movable mask which reduces heat load in the optical components downstream and also passes through slits (16.18 m from the undulator) in the optical hutch. The pink beam is monochromated by the liquid-nitrogen-cooled double-crystal monochromator (DCM) with Si(111) crystals with $\sim 2 \times 10^{-4}$ energy resolution. The two crystals have a variable gap, which moves the beam up after the DCM by a fixed value, 25 mm. The monochromatic X-ray beam is focused by a 40 nm rhodium-coated silicon toroidal mirror. Its reflective direction is downward and the beam is focused into 190 μm (H) × 15 μm (V) at the sample position (30 m). When the beam bypasses the mirror, its size is 2.95 mm (H) × 0.59 (V) mm. Then users can choose other optics such as the Fresnel zone plate in the experimental hutch. Main beamline parameters are listed in Table 2.

Fig. 3 displays a typical set-up for CDI in transmission geometry mode. A sample chamber is designed to mount on the diffractometer, and its inside is shown in the inset. The centre of the six-axis diffractometer is located at the mirror focal point. A pinhole defines the size of the coherent X-ray beam. Two guard slits reduce the parasitic scattering from the pinhole, and also reduce the background

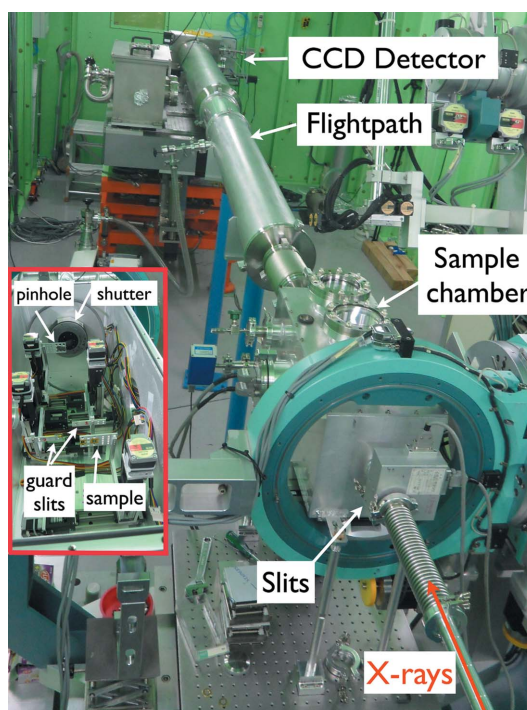


Figure 3

Typical transmission geometry set-up for CDI in the 9C experimental hutch. The X-ray beam passes into the sample chamber as shown by the red arrow and illuminates the sample, and the diffracted X-rays fly through the flight path. The direct beam is blocked at the beam-stop (not shown) and the signals are detected by the CCD. The inset displays the inside of the chamber, but the beam direction is from top to bottom (opposite to that in the main panel) for a clearer view.

of the scattered signals to the charge coupled device (CCD) detector. A Uniblitz X-ray shutter, XRS16 (16 mm-diameter opening, PtIr shutter blade, and 25 ms opening time), is installed in front of the pinhole and is synchronized to the CCD enable-signal-out. By controlling the shutter opening time, one can acquire unsaturated signal near the direct beam, *i.e.* signal for low momentum transfers having the shape information of the sample. We plan to upgrade the shutter to an XRS6 with 5 ms opening time. Two flight paths of lengths 1.7 m and 1.9 m are connected to the sample chamber and a beam-stop chamber. The beam-stop chamber, with kapton windows, is in front of the CCD detector and is installed with the beam-stop with two translational motions. This transmission geometry is useful not only for CDI but also for XPCS depending on the samples.

The beamline provides two two-dimensional detectors: Princeton Instruments PIXIS-XO CCD (pixel size $13\ \mu\text{m} \times 13\ \mu\text{m}$, image area $13.3\ \text{mm} \times 13.3\ \text{mm}$) and Dectris Pilatus 1M (pixel size $172\ \mu\text{m} \times 172\ \mu\text{m}$, image area $169\ \text{mm} \times 179\ \text{mm}$). Two flight paths allow users to choose the position of the detectors depending on the interests of the wavevector region and the required resolution of the experiments. The beam path, the sample chamber and the beam-stop chamber are under vacuum (10^{-2} torr) to reduce air scattering. Bragg CDI has been also carried out in the beamline with the six-axis diffractometer.

The diffractometer and all motors in the experimental hutch are controlled by the *SPEC* software (Swislow, 2004). For the general X-ray scattering users, *SIXC* in *SPEC* software is installed to manipulate the diffractometer. Two sets of XHA filters and Huber slits, ion chambers as intensity monitors, and a Cyberstar 2000 scintillation detector are available. A 100 MHz FMB Oxford avalanche photodiode (APD) has also recently been made available for possible XPCS measurements with the reflection geometry.

For coherence preservation of X-ray beams, the beamline avoids graphite filters or diamond windows which are useful for reducing heat load in the photon transfer line; it only comes with a polished beryllium window at the entrance of the experimental hutch. General scattering experiments usually use the six-axis Huber diffractometer with the focused X-ray beam. The diffractometer and optical tables at the downstream end are used for coherent X-ray experiments depending on the experimental geometries; X-ray beam can bypass a focusing mirror. The longest sample-to-detector distance available is ~ 6 m.

The design performance of the 9C beamline can be estimated using equation (3.2.1) of the National Synchrotron Light Source-II (NSLS-II) Conceptual Design Report (Podobedov, 2006); the equation shows that photon intensity for imaging is inversely proportional to

measurement time and (spatial resolution)³. Because PLS-II 9C has 10^3 times less coherent flux than that of NSLS-II, it could have either a spatial resolution of about ten times worse or measurement time 10^3 times longer than that of NSLS-II. For example, while NSLS-II has 1 nm resolution for internal imaging of $1\ \mu\text{m}^3$ amorphous gold with a 4 min (unfocused) X-ray exposure, PLS-II 9C has 10 nm resolution for the same amount of time.

3. Facility access

PLS-II accepts user beam time proposals (two terms before summer and one term after summer every year) through its web site (<http://pal.postech.ac.kr>). Three kinds of proposals are available: (i) general proposals, which can only be effective for one term and must be open to the public; (ii) long-term proposals, which last for six terms and are also open to the public [general proposals and long-term proposals should be applied at designated times (three times per year)]; (iii) urgent request proposals, which can be applied at any time; after submitting a request, users should contact the corresponding beamline managers to explain the urgency and to check the availability of the beamline.

4. Highlights

CDI with transmission geometry on a star-shaped Au test sample was carried out to demonstrate the performance of the beamline. The micrometre-sized Au sample was prepared with electron beam lithography on a SiN membrane, and its thickness was 70 nm. The sample was put in the sample chamber, shown in Fig. 3. The storage-ring current was 125 mA for the experiments in this section. An X-ray beam of 5.36 keV was defined by the slits at 16.18 m (Fig. 1) to $300\ \mu\text{m} \times 300\ \mu\text{m}$ and focused (but not fully optimized) by the toroidal mirror to $200\ \mu\text{m}$ (H) \times $80\ \mu\text{m}$ (V) at the sample position (30 m) or the focal point. A pinhole of diameter $10\ \mu\text{m}$ was placed at the entrance of the sample chamber to define the final clean-cut beam. The pinhole was made by focused ion beam on $25\ \mu\text{m}$ -thick tantalum foil. The guard slits of thickness $127\ \mu\text{m}$ positioned between the sample and the pinhole reduced the background signal and allowed a better signal-to-noise ratio to be obtained. Their edges were polished.

The measured coherent X-ray diffraction data are illustrated in Fig. 4(a). One quarter of the two-dimensional image was blocked by the beam stop, and the final data were obtained by patching the data in the other areas centrosymmetrically. A user detector, Princeton

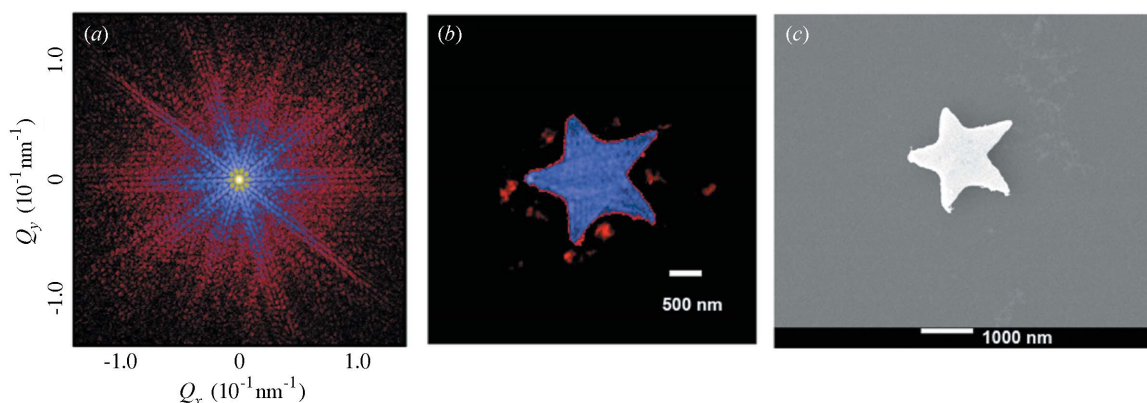


Figure 4 (a) Patched coherent X-ray diffraction data from a star-shaped Au sample (see text). (b) Reconstructed image and (c) SEM image of the Au sample.

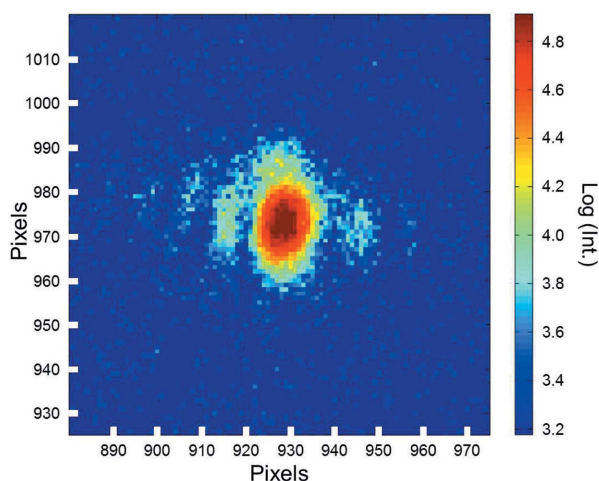


Figure 5
Bragg CDI of a ZSM-5 single crystal at (200) Bragg angle.

Instrument PI-LCX, of pixel size $20\ \mu\text{m} \times 20\ \mu\text{m}$ and chip size $26.8\ \text{mm} \times 26\ \text{mm}$, was used for this experiment. The image reconstruction was performed using a hybrid input–output algorithm (Fienup, 1982, 1987; Elser, 2003), and its result is shown in Fig. 4(b). The reconstructed image agrees well with the scanning electron microscopy (SEM) image in Fig. 4(c). Its half-period resolution is about 25 nm.

The Bragg coherent X-ray diffraction experiment was carried out in reflection geometry mode with the six-axis diffractometer. The sample, a 2 μm -sized ZSM-5 zeolite crystal, was attached to a silicon substrate by chemical bonding (Cha *et al.*, 2013). An X-ray of energy 9.2 keV illuminated the isolated sample and gave the coherent diffraction pattern at (200) Bragg angle shown in Fig. 5. The PI-LCX detector was set about 2 m away from the sample and measured the image for 480 s. The fringe patterns on the sides of the central peak are related to the sample shape and its size.

5. Conclusions

The PLS-II 9C beamline at PAL was designated for coherent X-ray scattering experiments in 2012 and is currently in operation with domestic user groups for CDI and XPCS. Its capability has been demonstrated by the experimental results shown above. PLS-II currently operates its top-up mode with <150 mA, and it will increase

its ring current to 400 mA in 2014, which will reduce data acquisition time and offer better resolution for CDI and XPCS.

Woul-Woo Lee, Chae-Soon Lee, Hyo-Yun Kim, Young-Duck Yun, In Deuk Seo and Seung Nam Kim are gratefully acknowledged for their mechanical and electrical assistance to the beamline construction and operation. The authors also thank Dr Yongsam Kim and Sang Tae Jung for discussions. This work was supported by the MSIP (Ministry of Science, ICT and Future Planning).

References

- Cha, W., Jeong, N. C., Song, S., Park, H. J., Thanh Pham, T. C., Harder, R., Lim, B., Xiong, G., Ahn, D., McNulty, I., Kim, J., Yoon, K. B., Robinson, I. K. & Kim, H. (2013). *Nat. Mater.* **12**, 729–734.
- Chapman, H. N. & Nugent, K. A. (2010). *Nat. Photon.* **4**, 833–839.
- Eisebitt, S., Lüning, J., Schlotter, W. F., Lörger, M., Hellwig, O., Eberhardt, W. & Stöhr, J. (2004). *Nature (London)*, **432**, 885–888.
- Elser, V. (2003). *J. Opt. Soc. Am. A*, **20**, 40–55.
- Fienup, J. R. (1982). *Appl. Opt.* **21**, 2758–2769.
- Fienup, J. R. (1987). *J. Opt. Soc. Am. A*, **4**, 118–123.
- Miao, J., Charalambous, P., Kirz, J. & Sayre, D. (1999). *Nature (London)*, **400**, 342–344.
- Mochrie, S. G. J., Mayes, A. M., Sandy, A. R., Sutton, M., Brauer, S., Stephenson, G. B., Abernathy, D. L. & Grübel, G. (1997). *Phys. Rev. Lett.* **78**, 1275–1278.
- Podobedov, P. (2006). NSLS-II Conceptual Design Report. Brookhaven National Laboratory, New York, USA.
- Shapiro, D., Thibault, P., Beetz, T., Elser, V., Howells, M., Jacobsen, C., Kirz, J., Lima, E., Miao, H., Neiman, A. M. & Sayre, D. (2005). *Proc. Natl Acad. Sci. USA*, **102**, 15343–15346.
- Shin, S., Kwon, S., Kim, D.-T., Kim, D.-E., Kim, M., Kim, S.-H., Kim, S.-C., Kim, J., Kim, C., Park, B., Park, S.-S., Park, S.-J., Park, E., Son, Y., Yoon, J., Lee, B., Lee, E., Lee, J.-W., Lee, H.-S., Joo, Y., Choi, J., Ha, T., Hwang, W., Hwang, I., Lee, J.-Y., Oh, B., Lee, C.-H., Lee, H.-S., Kim, J.-Y., Hwang, J., Nam, S. & Cho, M. (2013). *J. Instrum.* **8**, P01019.
- Stadler, L. M., Gutt, C., Autenrieth, T., Leupold, O., Rehbein, S., Chushkin, Y. & Grübel, G. (2008). *Phys. Rev. Lett.* **100**, 245503.
- Sutton, M., Mochrie, S. G. J., Greytak, T., Nagler, S. E., Berman, L. E., Held, G. A. & Stephenson, G. B. (1991). *Nature (London)*, **352**, 608–610.
- Swislow, G. (2004). *Spec.*, <http://www.certif.com/content/Spec/>.
- Tanaka, T. (undated). *SPECTRA – a synchrotron radiation calculation code*, <http://radiant.harima.riken.go.jp/spectra/>.
- Welnak, C., Chen, G. J. & Cerrina, F. (1994). *Nucl. Instrum. Methods Phys. Res. A*, **347**, 344–347.
- Williams, G. J., Pfeifer, M. A., Vartanyants, I. A. & Robinson, I. K. (2003). *Phys. Rev. Lett.* **90**, 175501.
- Wochner, P., Gutt, C., Autenrieth, T., Demmer, T., Bugaev, V., Ortiz, A. D., Duri, A., Zontone, F., Grübel, G. & Dosch, H. (2009). *Proc. Natl Acad. Sci.* **106**, 11511–11514.